Adaptive Dictionary-Based Spatio-Temporal Flow Estimation for Echo PIV

Ecaterina Bodnariuc*[1], Arati Gurung[2], Stefania Petra[1]**, and Christoph Schnörr*[1]

[1] Image and Pattern Analysis Group, University of Heidelberg, Germany
ecaterina.bodnariuc@iwr.uni-heidelberg.de,
{petra,schnoerr}@math.uni-heidelberg.de
[2] Laboratory for Aero and Hydrodynamics (3ME-P&E), Delft University of Technology, The Netherlands
a.gurung@tudelft.nl

Abstract. A novel approach is presented to detect the trajectories of particles by combining (a) adaptive dictionaries that model physically consistent spatio-temporal events, and (b) convex programming for sparse matching and trajectory detection in image sequence data. The mutual parametrisation of these two components are mathematically designed so as to achieve provable convergence of the overall scheme to a fixed point. While this work is motivated by the task of estimating instantaneous vessel blood flow velocity using ultrasound image velocimetry, our contribution from the optimization point of view may be of interest also to related pattern and image analysis tasks in different application fields.

Keywords: motion estimation, fixed point algorithm, adaptive dictionaries, sparse representation, sparse error correction, Echo PIV

1 Introduction

Overview. *Ultrasound Image Velocimetry (Echo PIV)* has become a recent focus of research in view of its potential for clinical applications. Specifically, instantaneous blood flow rates and wall shear stress measurements with low-cost hardware are of particular interest, e.g. in connection with atherosclerosis-related screening [1].

Currently available sensors, however, severely limit the spatial and temporal resolution of measurements. Computational cross-correlation techniques, adopted from traditional laser-based imaging and PIV techniques in different fields of experimental fluid mechanics [2], suffer from a poor quality of reconstructed image sequences and from a high level of noise. Moreover, by using established cross-correlation methods, it is neither straightforward to replace in a mathematically consistent way frame-by-frame processing by spatio-temporal

* EB and CS appreciate financial support by the German Research Foundation (DFG).
** SP acknowledges financial support by the Ministry of Science, Research and Arts, Baden-Württemberg, within the Margarete von Wrangell postdoctoral lecture qualification program.

image analysis in order to aggregate motion information over an entire image sequence, nor to take into account physical principles governing the imaged fluid flow.

In this paper we present a novel approach that directly addresses these shortcomings in terms of adaptive spatio-temporal dictionaries of particle trajectories. These dictionaries are based on a basic physical model of vessel blood flow and are integrated into a standard sparse convex programming framework.

Related Work, Contribution. Research in connection with Echo PIV concerns (i) sensor design and (ii) image analysis. Since research on sensor design is rapidly evolving [3,4], we ignore this inverse modelling aspect and focus on (ii) in terms of a *mathematical abstraction based on "particles", to be understood as coefficients of a basis expansion, that discretises a realistic imaging operator in our future work.*

Concerning (ii) image analysis, standard PIV techniques [2] are the prevailing approach for applying Echo PIV [1]. In this paper, we propose a radically different approach with the following objectives:

1. Any imaging operator model discretized by suitable basis functions can be incorporated later on.
2. Particle trajectories are detected by a comprehensive spatio-temporal analysis of entire image sequences in terms of dictionaries of trajectories. This copes better with noise in comparison to techniques that merely analyse subsequent image pairs. Furthermore, physical models of vessel blood flow [5,6] can be directly exploited.
3. The computational costs for the aforementioned spatio-temporal analysis are subdivided by adapting a smaller collection of dictionaries until convergence.

While the novelty of our approach is obvious from the viewpoint of Echo PIV, our main contribution from the optimization point of view concerns the *consistent integration of adaptive dictionaries* into a standard sparse convex programming framework. This is accomplished by carefully modelling the mutual interaction of dictionary parametrization and sparse convex particle matching so as to obtain a provably converging fixed point scheme. These mathematical aspects of our approach might be of interest also to related computational image and pattern analysis tasks in different application fields.

Organization. The application and the corresponding imaging techniques are sketched in Section 2. Section 3 details the model-based definition of dictionaries together with the variational approach for motion estimation through particle trajectory detection. Section 4 provides a convergence analysis of the adaptive variational approach. Properties of our approach are validated experimentally in Section 5.

Basic Notation. We set $[n] = \{1, 2, \ldots, n\}$ for $n \in \mathbb{N}$. Vectors are column vectors and indexed by superscripts. $\langle x, z \rangle$ denotes the standard scalar product in $\mathbb{R}^n$, and $\|x\|_1 = \sum_{i=1}^n |x_i|$ and $\|x\| := \|x\|_2 = \sqrt{\sum_{i=1}^n x_i^2}$. $\mathbb{1} = (1, 1, \ldots, 1)^\top$ denotes the one-vector whose dimension will always be clear from the context. $\Delta_d = \{x \in \mathbb{R}^d_+ : \langle \mathbb{1}, x \rangle = 1\}$ denotes the probability simplex in $\mathbb{R}^d$.

2 Ultrasound Imaging and Echo PIV

We briefly sketch the state-of-the-art in imaging and motion analysis in Echo PIV, in order to highlight the novelty of our own methodological approach that differs from the established computational techniques in this field of application.

Particle Image Velocimetry (PIV). *PIV* is an optical method for measuring fluid flows. For the purpose of imaging, the fluid is seeded with particles that follow the flow dynamics. The region of interest is illuminated with a laser sheet and a high-speed camera takes successive images. In a subsequent step, a cross correlation technique is applied to every pair of two subsequent images and returns an estimate of the instantaneous velocity field. For a recent overview of the history of PIV techniques, we refer to [7].

Ultrasound Microbubble Imaging. *Echo PIV*, first introduced in [8], is a

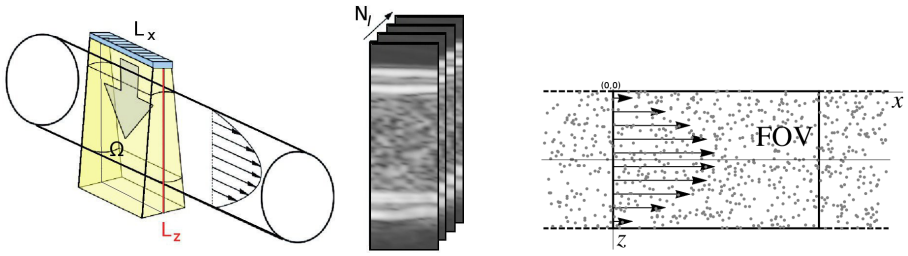

Fig. 1. A schematic representation of an Echo PIV setup. The left image, adapted from [1], overviews geometry and orientation of the transducer. Velocity is estimated from a sequence of B-mode images (middle). Flow motion is estimated from the motion of tracer particles injected in the medium (right), which follow the flow dynamics – here, a laminar and steady flow.

technique based on the same principles as PIV. Within Echo PIV, however, high-speed cameras are replaced by an *ultrasound transducer*. Thus, the technique can be applied to opaque media as well. Another major difference to optical 2D PIV is the generation of so-called *B-mode* 2D images, as sketched in Figures 1 and 2. Recording of the images is accomplished by the use of the *pulse-echo* methodology and by concatenating several line-by-line measurements, as depicted in Fig. 2. This severely limits the spatio-temporal resolution of flow measurements.

One way to overcome this problem is to replace multiple line measurements by a single *plane wave* illumination of the medium [3]. *Plane wave imaging* was very recently applied to Echo PIV [4] and allows for measuring higher velocities, since the frame rate is only limited by the propagation time of the waves, rather than by the number of consecutive measurements necessary to obtain a single B-mode image. *This motivates us to ignore inter-line delay in our work.*

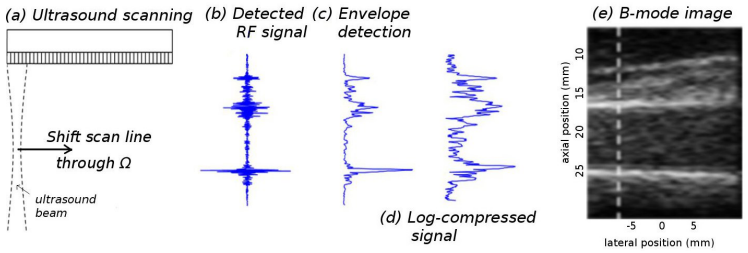

Fig. 2. B-mode imaging in Echo PIV: images are not recorded as snapshots, but are usually constructed line-by-line, due to the shifting of the ultrasound beam (a). The data – RF signals (b) – can be converted (offline) to so-called B-mode images (e) by means of envelope detection (c) and log compression (d). This scanning procedure results in a blurred image due to moving particles between consecutive measurements.

Motion Estimation. Standard Echo PIV setups estimate the velocity field by processing the sequence of B-mode images using local cross-correlation of subsequent image pairs, as in conventional PIV [7,9]. Such PIV methods fail to

(i) exploit the entire spatio-temporal context of a corresponding volume of image sequence data, and
(ii) take into account physical prior knowledge in a mathematically more principled way.

Our present work addresses both aspects for the specific setting of Echo PIV as summarized in Section 1.

3 Spatio-Temporal Motion Model and Estimation

3.1 Dictionary of Moving Particles

As mentioned in Section 2, in Echo PIV experiments images are created by merging vertical segments of the field of view (FOV) recorded at different time steps. As a consequence the frame rate is low and the maximal velocity that can be measured is limited. In the present work we consider a different acquisition protocol motivated by current research on image acquisition [3,4] in which the whole image/frame is recorded at the same point in time.

With index n we label the image of the FOV recorded at time $\tau_n = (n-1)\,\Delta t$, $n \in [N_I]$, where N_I is the total number of frames. All images have size $L_x \times L_z$ in length units or $l_x \times l_z$ in pixels. We introduce a 2D rectangular grid with lattice spacing $\Delta x = L_x/l_x$, $\Delta z = L_z/l_z$ in x and z respectively in the plane of FOV, induced by discrete pixel representation of images.

Below we describe how to build a flow dictionary corresponding to a laminar and steady flow with maximal velocity along the cylinder axis equal to v_m.

Dictionary of a single velocity profile. The dictionary of trajectories D is a sparse matrix with binary entries $\{0, 1\}$ and it describes the position of

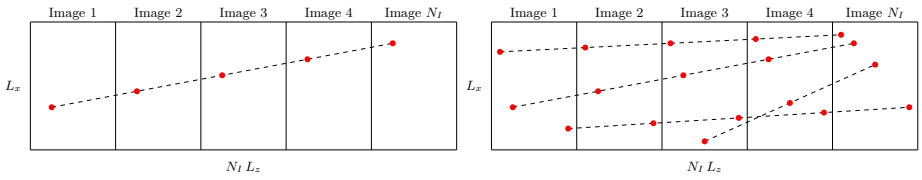

Fig. 3. Each column of the dictionary D is an image of an undersampled discrete line, and describes a possible trajectory in the N_I acquired images concatenated along the tube axis (left). Each such column depends on the discretization of Ω, acquisition process and flow model. Here the Poiseuille flow model leads to straight lines. The input data (right) is given by all N_I frames concatenated along the tube axis. The problem is to *sparsely* match *imaged* particles to trajectories in D parametrized by the unknown maximal velocity v_m.

particles at time τ_n, $n \in [N_I]$ relative to the FOV. Each column in D is associated to the trajectory of a single particle j, $j \in [N_P]$, where N_P denotes the number of particles. The number of columns in D equals the number of possible trajectories. Due to the discretization, in the limit when a particle is located at all grid points, there is an upper bound for $N_P < l_x\, l_z + (N_I - 1)\, \Delta t\, v_m\, l_x L_x / l_z$. The number of rows in D is independent of v_m and equals $N_I l_x l_z$.

According to the adopted model sketched in Figure 1 (right panel), the motion of particle j with initial coordinates (x_1^j, z_1^j) at time τ_1 is governed by

$$\begin{cases} x_n^j = x_1^j + (n-1)\Delta t\, v_m \left(1 - \left(\frac{r^j}{R}\right)^2\right), \\ z_n^j = z_1^j = \ const. \end{cases} \tag{1}$$

where $r^j = |z_1^j - R|$, $z_1^j \in [0, 2R]$ is the distance from the axis and R the inner radius R of the cylinder.

If at time τ_n particle j is present in the FOV, i.e. $x_n^j \in (0,\, L_x]$, then its pixel coordinates in image n is $(m_{x_n}^j, m_{z_n}^j)$, where $m_{x_n}^j = \lceil \frac{x_n^j}{\Delta x} \rceil$, $m_{x_n}^j \in [l_x]$ ($\lceil a \rceil$ is the smallest integer larger then a) and since coordinates z remain unchanged over time we set z_1^j, $\forall\, j \in [N_P]$, to have the form

$$z_1^j = z_n^j = (m_{z_n}^j - \frac{1}{2})\Delta z, \tag{2}$$

$m_{z_n}^j \in [l_z]$. Further, we select the row index

$$i_n^j = (n-1)\, l_x\, l_z + m_{z_n}^j\, l_x - m_{x_n}^j + 1 \tag{3}$$

and define the entries in the j column of the dictionary as

$$D_{ij} = D_{ij}(v_m) = \begin{cases} 1, & \text{if } i = i_n^j, \\ 0, & \text{otherwise.} \end{cases} \tag{4}$$

We stress the fact that, with all discretization parameters fixed, *a dictionary* D of particle trajectories corresponding to a single velocity profile (1) *is parametrized by the single scalar maximal velocity* v_m.

The above definition implies that the number of non vanishing entries in any column j does not exceed the number of images N_I. This is consistent with the physical picture that a particle appears only once in a measured image, or it does not appear at all. We note that two columns $D_{\bullet,j}, D_{\bullet,j'}$ will be equal if and only if the initial coordinates for two different particles are equal, i.e. $(x_1^j, z_1^j) = (x_1^{j'}, z_1^{j'})$. Consequently D will not contain redundant (equal) columns. Another consequence is the orthogonality of the columns of D, as formally stated next.

Proposition 1. *For any two columns $D_{\bullet,j}$ and $D_{\bullet,j'}$ in D corresponding to particles with initial coordinates (x_1^j, z_1^j) and $(x_1^{j'}, z_1^{j'})$ we have*

$$\langle D_{\bullet,j}, D_{\bullet,j'} \rangle = 0 \quad \Longleftrightarrow \quad (x_1^j, z_1^j) \neq (x_1^{j'}, z_1^{j'}). \tag{5}$$

Proof. We show $\langle D_{\bullet,j}, D_{\bullet,j'} \rangle \neq 0 \iff (x_1^j, z_1^j) = (x_1^{j'}, z_1^{j'})$.
"$\Leftarrow$" Clear, in view of (1) and the construction of D.
"$\Rightarrow$" Assume $\langle D_{\bullet,j}, D_{\bullet,j'} \rangle \neq 0$. We show that this implies $(x_1^j, z_1^j) = (x_1^{j'}, z_1^{j'})$. The assumption implies that there exists an index $i_n = i_{n'}$ such that $D_{i_{n'}\, j'} = D_{i_n\, j} = 1$, i.e. by (3)

$$n\, l_x\, l_z + m_{z_n}^j\, l_x - m_{x_n}^j = n'\, l_x\, l_z + m_{z_{n'}}^{j'}\, l_x - m_{x_{n'}}^{j'}. \tag{6}$$

From $m_{z_n}^j = \{1, \ldots, l_z\}$ and $m_{x_n}^j = \{1, \ldots, l_x\}$, we have $0 \leq m_{z_n}^j\, l_x - m_{x_n}^j \leq l_x\, l_z - 1$, and similarly for j', i.e. $0 \leq m_{z_{n'}}^{j'}\, l_x - m_{x_{n'}}^{j'} \leq l_x\, l_z - 1$. Dividing (6) through $l_x\, l_z$, we get

$$\underbrace{n}_{\in\mathbb{N}} + \underbrace{\frac{m_{z_n}^j\, l_x - m_{x_n}^j}{l_x\, l_z}}_{\in[0,1)\cap\mathbb{Q}} = \underbrace{n'}_{\in\mathbb{N}} + \underbrace{\frac{m_{z_{n'}}^{j'}\, l_x - m_{x_{n'}}^{j'}}{l_x\, l_z}}_{\in[0,1)\cap\mathbb{Q}} \tag{7}$$

from which we conclude $n = n'$ and $m_{z_n}^j\, l_x - m_{x_n}^j = m_{z_{n'}}^{j'}\, l_x - m_{x_{n'}}$. Rewriting the latter expression as

$$m_{z_n}^j = m_{z_n}^{j'} + (m_{x_n}^j - m_{x_n}^{j'})/l_x, \tag{8}$$

we infer $m_{x_n}^j - m_{x_n}^{j'} = 0$ as follows: The relation $|\, m_{x_n}^j - m_{x_n}^{j'}\, | \leq l_x - 1$, $m_{z_n}^j$, $m_{z_n}^{j'} \in \mathbb{N}$ and $n = n'$ implies $m_{x_n}^j = \lceil \frac{x_n^j}{\Delta x} \rceil$. Since this equality must hold for any Δx, we conclude $x_n^j = x_n^{j'}$.

As a consequence, (8) implies $m_{z_n}^j = m_{z_n}^{j'}$ and hence $z_1^j = z_1^{j'}$ by (2). This together with (1) and $x_n^j = x_n^{j'}$ finally implies $x_1^j = x_1^{j'}$. □

3.2 Variational Motion Estimation

Given noisy measurements F of particles $\{(x_n^j, z_n^j)\}_{j\in[N_P], n\in[N_I]}$ for a collection of N_I subsequent frames at points of time $\tau_n = (n-1)\Delta t$, $n \in [N_I]$, we set up an adaptive variational approach for localizing these particles in F.

To this end, we exploit the motion model (1) that describes particles' trajectories parametrized by the *unknown maximal velocity* v_m and *unknown initial coordinates* (x_1^j, z_1^j). Aggregating potential local detections over time in this way is our approach (i) to suppress noise, (ii) to discriminate particles from each other, and (iii) to estimate the unknown velocity v_m that is the ultimate goal from the viewpoint of the application area.

We make the reasonable assumption of knowing an interval

$$v_m \in [v_{\min}, v_{\max}], \quad v_{\min} > 0 \tag{9}$$

that contains the unknown parameter v_m. Every velocity value $v'_m \in [0, v_{\max}]$ defines a dictionary $D(v'_m)$ by (4) that exhaustively enumerates trajectories generated by (1) with $v_m = v'_m$, that could have been observed in the image sequence. If we knew the true velocity v_m, we could detect trajectories in the data F by sparsely matching $D(v_m)u$ to F, where u corresponds to a sparse indicator vector selecting active trajectories in $D(v_m)$.

Since v_m is not given, we have to estimate it from the data F as well. Since a single dictionary $D(v'_m)$ is quite large, setting up a collection of dictionaries

$$D(v) := \big(D(v_1), D(v_2), \ldots, D(v_d)\big), \qquad 0 < v_1 < v_2 < \cdots v_d < v_{\max} \tag{10}$$

with closely spaced values $\{v_i\}_{i\in[d]}$ is computationally infeasible. We therefore limit d to a reasonable value (see Section 5 for the setup) and *estimate* v_m *by an adaptive sequence of dictionaries* defined by a sequence of velocity vectors

$$D_{(k)} := D(v^{(k)}), \qquad v^{(k)} = (v_1^{(k)}, \ldots, v_d^{(k)})^\top \in [v_{\min}, v_{\max}]^d, \quad k \in \mathbb{N} \tag{11}$$

that localizes $v_m \in [v_1^{(k)}, v_d^{(k)}]$ in intervals of shrinking sizes: $|v_d^{(k)} - v_1^{(k)}| < |v_d^{(k-1)} - v_1^{(k-1)}|$. At each iterative step k, we match trajectories and data by solving

$$u^{(k)} := \operatorname*{argmin}_{u\in[0,1]^N} \|D_{(k)}u - F\|_1 + \frac{\alpha}{2}\|u\|^2 + \frac{1}{2\lambda}\|u - u^{(k-1)}\|^2, \qquad \alpha > 0, \lambda > 0. \tag{12}$$

We stress that nonnegativity constraints enforce *sparse recovery* without explicit sparse regularization [10]. In order to additionally cope with *sparse outliers* we decided to use an ℓ_1-based data/linear model discrepancy term, since minimizing $\|D_{(k)}u - F\|_1$ is better suited for sparse error recovery, see [11]. Subsequently, we subdivide $u^{(k)}$ into subvectors conforming to the structure (10) of $D_{(k)}$,

$$u^{(k)} = (u^{1,(k)}, \ldots, u^{d,(k)}), \tag{13}$$

and estimate v_m as convex combination of the velocity values $v^{(k)}$ defining the current dictionary $D_{(k)}$,

$$v_m^{(k)} := \sum_{i\in[d]} w_i^{(k)} v_i^{(k)} = \langle w^{(k)}, v^{(k)} \rangle, \quad w_i^{(k)} := \frac{1}{\|u^{(k)}\|_1}\|u^{i,(k)}\|_1, \quad i \in [d]. \tag{14}$$

Iteration step k is completed by updating the velocity vector

$$v^{(k+1)} = V_\tau(u^{(k)}, v^{(k)}), \quad v_i^{(k+1)} := v_m^{(k)} + \tau(v_i^{(k)} - v_m^{(k)}), \quad i \in [d], \tag{15}$$

with $\tau \in (0,1)$. In the next section, it is shown that for any choice of the parameters $\lambda > 0$ and $\tau \in (0,1)$, the sequence of *non-stationary* mappings (i.e. depending on k)

$$v^{(k)} \xrightarrow{\text{Eqn. (12)}} u^{(k)} \xrightarrow{\text{Eqn. (15)}} v^{(k+1)} \tag{16}$$

is a fixed point iteration that converges to a constant vector $v^{(\infty)} = v_m \mathbb{1}$, that constitutes the estimate of v_m. The quality of this estimate from the applied viewpoint as outlined in Section 2, will be assessed in Section 5.

4 Convergence Analysis

We next show the convergence of the scheme (16) under mild conditions. The proof reveals how the scheme can be modified from the viewpoint of the intended application without compromising convergence. We describe a promising variant in the next paragraph.

Convergence. We write for the proximal mapping $u^{(k-1)} \to u^{(k)}$ defined by (12)

$$u^{(k)} = P_\lambda f(u^{(k-1)}, v^{(k)}) := \operatorname{argmin}_u \, f(u, v^{(k)}) + \frac{1}{2\lambda}\|u - u^{(k-1)}\|^2, \tag{17a}$$

$$f(u, v^{(k)}) := \|D_{(k)}u - F\|_1 + \frac{\alpha}{2}\|u\|^2 + \delta_C(u), \quad C = [0,1]^N, \tag{17b}$$

$$e_\lambda f(u, v^{(k)}) := \inf_w f(w, v^{(k)}) + \frac{1}{2\lambda}\|w - u\|^2, \tag{17c}$$

in order to exhibit the parametrization by $v^{(k)}$ defining the dictionary (11). Eq. (17c) additionally introduces the Moreau envelope $e_\lambda f$ of f [12, Def. 1.22], that we need in the proof of Prop. 2 below.

Likewise, we regard the mapping $v^{(k)} \mapsto v^{(k+1)}$ defined by (15) as parametrized by $u^{(k)}$. These mutual dependencies of the sequences $(u^{(k)})_{k\in\mathbb{N}}$ and $(v^{(k)})_{k\in\mathbb{N}}$ and their convergence are addressed next.

Proposition 2. *Let the sequences $(u^{(k)})_{k\in\mathbb{N}}, (v^{(k)})_{k\in\mathbb{N}}$ be given by (12) and (15), respectively. Suppose the mapping $v \mapsto D(v)$ is continuous. Then, for any initializations $v^{(0)} \in [v_{\min}, v_{\max}]^d \subset \mathbb{R}^d_{++}$ and $u^{(0)} \in C$, the sequence $v^{(k)} \xrightarrow{k\to\infty} v^{(\infty)} = v_m^{(\infty)}\mathbb{1}$ converges to a constant vector as fixed point, and the sequence $u^{(k)} \xrightarrow{k\to\infty} u^{(\infty)} = \operatorname{argmin} f(u, v^{(\infty)})$ converges to the corresponding minimizer of f.*

Proof. The mapping (15) reads in view of (14)

$$V_\tau(u, v) = \tau v + (1-\tau)v_m\mathbb{1} = \big(\tau I + (1-\tau)\mathbb{1}w^\top(u)\big)v =: V_\tau(u)v. \tag{18}$$

We observe for *every* fixed $u \in C$:

(i) $w(u) \in \Delta_d$ and hence constant vectors $c\mathbb{1}$, $c > 0$, constitute fixed points: $V_\tau(u)(c\mathbb{1}) = \tau c\mathbb{1} + (1-\tau)\langle w(u), c\mathbb{1}\rangle \mathbb{1} = c\mathbb{1}$.
(ii) The matrix $V_\tau(u)$ has eigenvalues $\tau \in (0,1)$ with multiplicity $d-1$ and 1, where the constant vectors are the eigenvectors corresponding to the largest eigenvalue 1.

As a consequence, V_τ constitutes a contraction for any non-constant vector v, $\|V_\tau(u,v') - V_\tau(u,v)\| < \|v' - v\|$, *independent* of u. Conversely, if we fix *any* feasible v and consider any sequence $u^{(k)} \to u$, then we have $V_\tau(u^{(k)}, v) \to V_\tau(u,v)$ due to the continuity of $V_\tau(\cdot, v)$.

As a consequence of these properties, a variant of Banach's fixed point theorem [13, Prop. 1.2] asserts that the equation $v_u = V_\tau(u, v_u)$ has exactly one positive solution in the unit sphere $(S^{d-1} \cap [v_{\min}, v_{\max}]^d) \subset \mathbb{R}^d_{++}$ and that $v_{u^{(k)}} \to v_u$.

Next, we consider the mapping $u^{(k-1)} \mapsto u^{(k)}$, given by the proximal mapping (17), that is parametrized by $v^{(k)}$. We have to show convergence of the sequence of minima (17a), which is best covered by the epi(graphical)-convergence [12, Def. 7.1] of the sequence (17b) of functions $f^{(k)} := f(\cdot, v^{(k)})$, whose analysis simplifies due to f being proper, lower semicontinuous and (strongly) convex as follows.

By [12, Thm. 7.37], pointwise convergence $e_\lambda f^{(k)}(u) \to e_\lambda f^{(\infty)}(u)$ of the Moreau envelopes (17c) for some $\lambda > 0$, which holds due to the continuity of $v \mapsto D(v)$ by assumption, already yields epi-convergence of the sequence $f^{(k)}$ to $f^{(\infty)}$. This in turn assures by [12, Thm. 7.33] convergence of the unique minima $u^{(k)} \to u^{(\infty)}$, where uniqueness is due to the strict convexity of the objective function of (17a), and finally $u^{(\infty)} = \operatorname{argmin} f^{(\infty)}$. □

As a result, the sequence $v^{(k)}$ converges to a constant vector $v^{(\infty)} = v_m \mathbb{1}$ in connection with the convergence of minima $u^{(k)} \mapsto u^{(\infty)}$ that finally determines the constant v_m which is the estimate we are primarily interested in, by matching the dictionary $D(v^{(\infty)})$ to the given data F through minimizing $\|D(v^{(\infty)})u - F\|_1$.

Remark 1. The assumption of continuity of the mapping $v \mapsto D(v)$, made in Prop. 2, does not strictly hold true for our current implementation described in Section 3.1, but only "up to (small) discretization effects". Our experiments show however that this does not compromise convergence. A more refined discretization using smooth compactly supported basis functions will remove this (minor) deficiency in our future work.

Variants of the Estimation Scheme. The proof of Proposition 2 shows that the assertion holds for any smooth mapping

$$u^{(k)} \mapsto w^{(k)} = w(u^{(k)}) \in \Delta_d. \tag{19}$$

As a consequence, we can investigate alternatives to the mapping (14). Attractive candidates are mappings that are more sensitive to the subvector $u^{i,(k)}$ in (13)

with maximal support $\max_{i\in[d]} \|u^{i,(k)}\|_1$. A natural candidate for such a smooth mapping is

$$w_i^{(k)} := \frac{1}{\sum_{j\in[d]} e^{s_j/\varepsilon}} e^{s_i/\varepsilon}, \quad s_i := \|u^{i,(k)}\|_1, \quad \varepsilon > 0, \quad i = 1, 2, \ldots, d. \tag{20}$$

This results in a strictly positive vector $w^{(k)} \in \Delta_d$ that, for $\varepsilon \to 0$, concentrates its mass at the component $i \in [d]$ corresponding to $\max_{i\in[d]} \|u^{i,(k)}\|_1$.

We summarize the performance of this variant in numerical experiments in Section 5.

5 Numerical Experiments

In this section, we illustrate the performance of our approach (see Section 3 and Alg. 1 below, for a compact summary), in noisy and non-noisy environments.

Experimental Setup. The experimental verification was done using data simulated as follows.

(a) first, randomly distribute a fixed number of microbubbles in the cross section of a tube with length L (100cm) and radius R (5cm);
(b) select an arbitrary value for v_m^* between $v_{min} = 0.001$ and $v_{max} = 5$;
(c) calculate the position of every microbubble according to Eq. (1) at each time step $\tau_n = (n-1)\Delta t$, $\Delta t = 0.2s$;
(d) scan simultaneously the field of view $\Omega = [0, L_x] \times [0, L_z]$ at each time τ_n and store $N_I = 20$ binary 2D images of size $l_x \times l_z$ (in pixels) and microbubbles position therein. $L_x = L_z = 10$ cm and $l_x = l_z = 100$;
(e) sort all N_I images and form the larger image $F_{ideal} =: F$ of size $l_x \times N_I l_z$ (see Figure 4);
(f) add noise to mimic ghost particles or error in the position of particles in the form of outliers or perturbing positions in a random direction of random particles. The amount of noise is given by

$$\#\text{ fraction of corrupted entries } = \frac{\|F_{ideal} - F_{noise}\|_1}{2\|F_{ideal}\|_1}.$$

We set the particle density to 10 particles/cm. For practical reasons we precompute and store in advance dictionary blocks corresponding to a single velocity profile for all velocity values in $[v_{min}, v_{max}]$ in steps of $\Delta v = 0.001$. The velocity resolution on this particular grid is of the order of Δv. Thus dictionary blocks $D(v_1)$ and $D(v_2)$ corresponding to v_1 and v_2 coincide if $|v_1 - v_2| < \Delta v$.

Optimization. For the two proposed variants mapping velocities (according to (14) or (20)), we run Alg. 1 below until the accuracy Δv was reached. The large-scale optimization task of Alg. (1) is the application of the proximal mapping and solving (12) at each iteration. To perform this task we currently use the CVX package for *disciplined convex programming* [14]. The average runtime for solving (12) is 5 minutes. Currently each D is a *highly sparse* $\left(2 \cdot 10^5\right) \times \left(N_P(v_i^k) \cdot d\right) \approx 2\cdot$

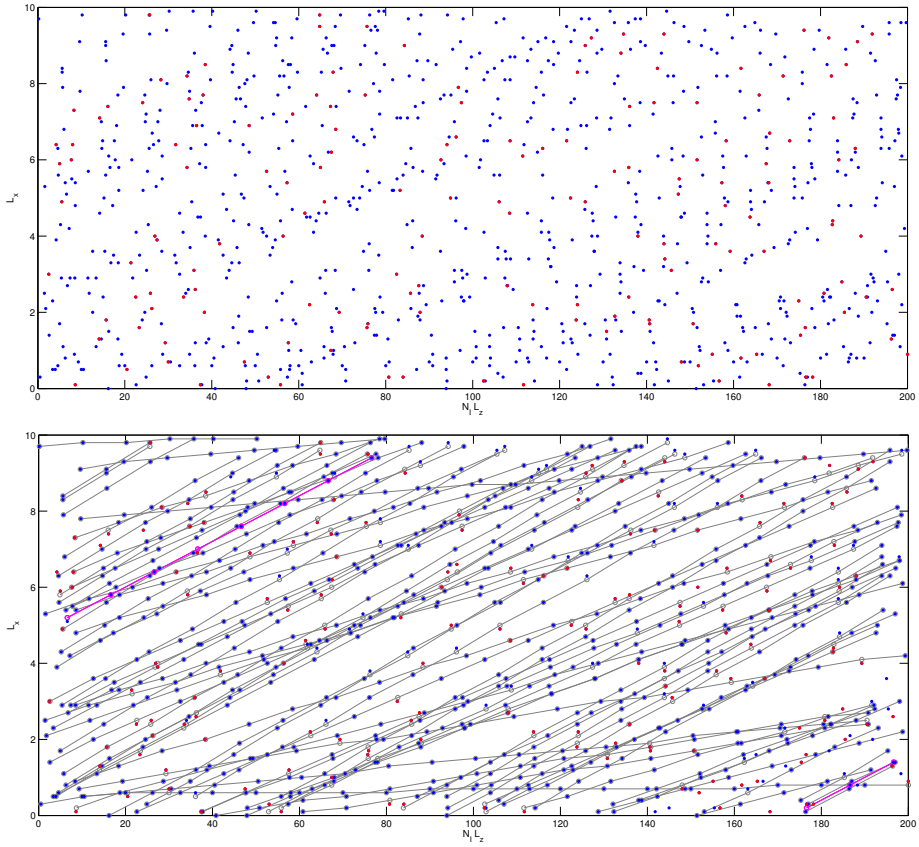

Fig. 4. Typical input (top) and output (bottom) of Alg. 1, but here using only 1% of the actual particle density for the purpose of visualization (better viewed in color). 20% (red dots) of input data are corrupted. All points should ideally belong to 84 unknown trajectories. Our proposed algorithm assigns microbubbles in the input frames to particle trajectories from a sparsifying dictionary. Correctly matched trajectories are displayed by thin black lines, wrong ones with magenta. The slopes of matched trajectories yield the velocity of each particle. Quantitative performance statistics for the full data sets are listed in Table 1.

$10^5 \times 10^6$ matrix, with $d = 11$ and $i \in [d]$. Each N_P depends on each velocity value v_i^k and $N_P(v_i^k) < l_x\, l_z + (N_I - 1)\, \Delta t\, v_i^k\, l_x L_x / l_z = 10^5 + 38 v_i^k$. For processing real data a dedicated numerical optimization algorithm is necessary as CVX cannot handle much larger problem sizes. We emphasize that by ignoring the quadratic terms in (12) the problem can be recast as a linear program. Thus (12) can be seen as a perturbed linear program. Our future work from the algorithmic point of view will exploit this fact along with the structure and sparsity of D consisting of d building blocks having each orthogonal columns due to Proposition 1.

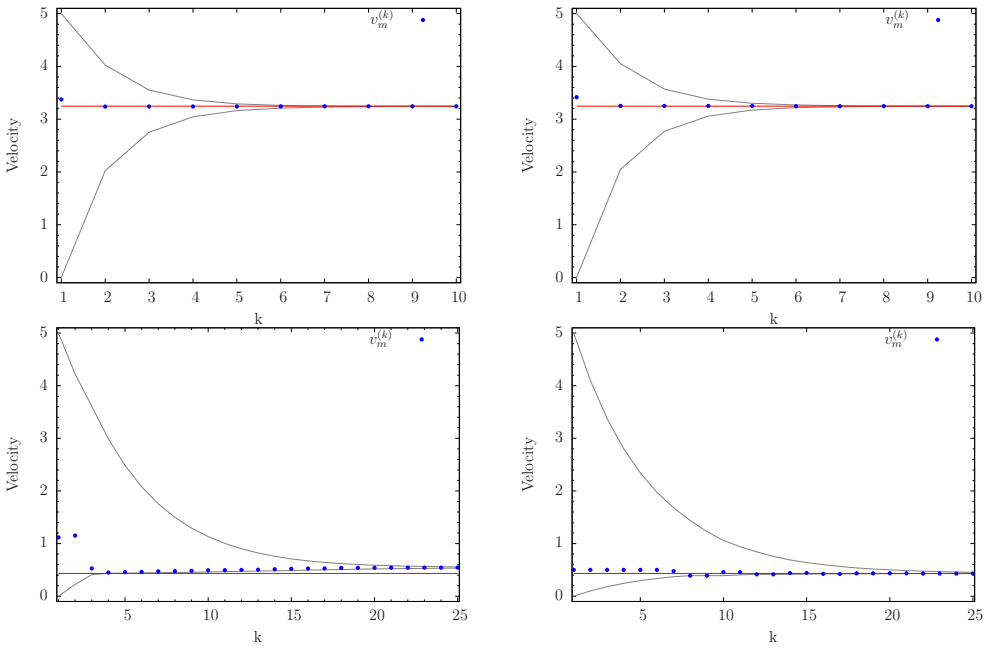

Fig. 5. Convergence performance of the fixed point Alg. 1 and its two variants for 20% noise, for *large* ($v_m^* = 3.2463$, top row) and *small* true (unknown) velocity ($v_m^* = 0.4321$, bottom row). Both variants of the algorithm for estimating v_m^* converged in 10 (top) and 25 (bottom) iterations. However, computing the weights w_i according to (20) based on the softmax function – *softmax-weights* – (right) leads to a more accurate estimate of v_m^* than computing weights according to (14) – ℓ_1*-weights* – (left). Further numerical values are given in Table 1 based on averaged results over 20 runs.

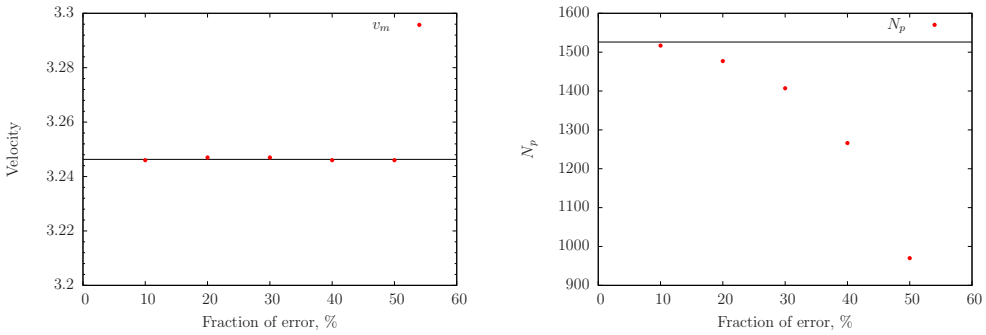

Fig. 6. Estimating the velocity v_m^* via Alg. 1 is robust (left) to corrupting a large fraction of the input data, although the fraction of correctly detected trajectories decreases (right). This fraction suffices to define a "correct" dictionary $D(v^{(k)})$ due to the convergence of $v^{(k)}$ to a uniform vector $v_m \mathbb{1}$. Results are consistent for different values of $\tau \in [0.4, 0.8]$, $\tau \in [0.2, 0.4]$ and $\varepsilon \in \{50, 100, 150, 200\}$.

Algorithm 1: Fixed Point Algorithm with two variants of mapping velocities according to (14) or (20).

Data: concatenated frames F, $d \in \mathbb{N}$ initial estimates for velocity profiles $v^{(1)} = (v_1^{(1)}, \dots, v_d^{(1)})$, parameters $\Delta v > 0$, $\lambda > 0$, $\alpha > 0$, $\varepsilon > 0$, $\tau \in (0,1)$

Result: v_m, N_p

$k = 1$;

while $|v_d^{(k)} - v_1^{(k)}| < \Delta v$ **do**

$D_{(k)} = (D(v_1^{(k)}),\ D(v_1^{(k)}),\ \dots,\ D(v_d^{(k)}))$;

$u^{(k)} = \arg\min_{u \in [0,1]} \| D_{(k)}\, u - F \|_1 + \frac{\alpha}{2}\|u\|^2 + \frac{1}{2\lambda}\|u - u^{(k-1)}\|^2$;

Compute weights from (14) / (20): ;

$\forall j \in [d]\colon \quad w_j^{(k)} = \frac{s_j}{\|u^{(k)}\|_1},\ s_j := \|u^{j,(k)}\|_1 \quad / \quad w_j^{(k)} := \frac{1}{\sum_{\ell \in [d]} e^{s_\ell/\varepsilon}} e^{s_j/\varepsilon}$;

$v_m^{(k)} = \sum_{i \in [d]} w_i^{(k)}\, v_i^{(k)}$;

$\forall j \in [d]\colon \quad v_j^{(k+1)} = v_m^{(k)} + \tau(v_j^{(k)} - v_m^{(k)})$;

$k = k + 1$;

$v_m = v_m^{(k)}, \qquad N_P = \|u^{(k)}\|_0$;

Results and Discussion. Fig. 4 illustrates the detection and particle trajectories after convergence to the fixed point according to Prop. 2. The convergence behavior is depicted by Fig. 5 along with a discussion in the caption. Finally Fig. 6 demonstrates a remarkable robustness of our approach against data noise over a wide range of values of the parameters $\tau \in (0,1)$, $\lambda > 0$ and ε in (20), due to the aggregation of all information over the entire spatio-temporal volume.

6 Conclusion

We have reformulated the velocity estimation problem for laminar and steady flow within Echo PIV experiments as a sparse and global spatio-temporal estimation problem, using a physical fluid flow model. The input data is the whole image sequence which is assumed to be well approximated by the sum of few elements from a flow dictionary. Since the dictionary is parametrized by the unknown velocity profile, we propose to update the dictionary in each iteration, obtaining an iterative algorithm which further refines the unknown quantity. We showed convergence to a fixed point of the overall scheme under weak assumptions to a sparsifying dictionary that robustly estimates velocity even in the presence of high levels of noise. Numerical examples demonstrate this robustness, convergence and estimation accuracy of our approach.

Further work will concentrate on adapting the dictionary using more general physical fluid flow models, and on incorporating models of the real imaging sensor along with proper discretization.

	$v_m^* = 3.2463;\quad N_p^* = 1526;\quad \tau = 0.4$					
	0 %		10 %		20 %	
	v_m	N_p	v_m	N_p	v_m	N_p
ℓ_1-weights	3.2437 ± 0.003	1526	3.2438 ± 0.0003	1513 ± 3	3.2437 ± 0.005	1478 ± 8
softmax-weights	3.2450 ± 0.006	1526	3.2456 ± 0.007	1519 ± 3	3.2460 ± 0.0006	1493 ± 5
	$v_m^* = 0.4321;\quad N_p^* = 1035;\quad \tau = 0.8$					
	0 %		10 %		20 %	
	v_m	N_p	v_m	N_p	v_m	N_p
ℓ_1-weights	0.4416 ± 0.016	1031	0.4688 ± 0.0037	754 ± 11	0.5291 ± 0.0227	360 ± 64
softmax-weights	0.4300 ± 0.020	1035	0.4296 ± 0.0007	1032 ± 2	0.4299 ± 0.0008	731 ± 24

Table 1. Estimated velocity and number of particles for ideal and noise data. The velocity value to be estimated is v_m^*. The number of true trajectories is N_p^*. We averaged results over 20 runs. Velocity estimates are stable against noise, and the results reveal better estimates for the softmax-weights in the case of small velocities.

References

1. Poelma, C., van der Mijle, R.M.E., Mari, J.M., Tang, M.X., Weinberg, P.D., Westerweel, J.: Ultrasound Imaging Velocimetry: Toward Reliable Wall Shear Stress Measurements. European Journal of Mechanics - B/Fluids **35** (2012) 70–75
2. Raffel, M., Willert, C., Wereley, S., Kompenhans, J.: Particle Image Velocimery – A Practical Guide. Springer (2007)
3. Schiffner, M.F., Schmitz, G.: Fast Image Acquisition in Pulse-Echo Ultrasound Imaging using Compressed Sensing. In: Ultrasonics Symposium (IUS), 2012 IEEE International, IEEE (2012) 1944–1947
4. Rodriguez, S., Jacob, X., Gibiat, V.: Plane Wave Echo Particle Image Velocimetry. In: Proceedings of Meetings of Acoustics, POMA 19. (2013)
5. Womersley, J.: Method for the calculation of velocity, rate of flow and viscous drag in arteries when the pressure gradient is known. J. Physiol. **127** (1955) 553–563
6. Sutera, S., Skalak, R.: The History of Poiseuille's Law. Ann. Rev. Fluid Mech. **25** (1993) 1–19
7. Adrian, R.J.: Twenty Years of Particle Image Velocimetry. Experiments in Fluids **39**(2) (2005) 159–169
8. Kim, H., Hertzberg, J., Shandas, R.: Development and Validation of Echo PIV. Exp. Fluids **36**(3) (2004) 455–462
9. Westerweel, J.: Fundamentals of Digital Particle Image Velocimetry. Measurement Science and Technology **8**(12) (1997) 1379–1392
10. Slawski, M., Hein, M.: Sparse Recovery by Thresholded Non-Negative Least Squares. In: Proc. NIPS. (2011) 1926–1934
11. Candès, E.J., Tao, T.: Decoding by Linear Programming. IEEE Transactions on Information Theory **51**(12) (2005) 4203–4215
12. Rockafellar, R., Wets, R.J.B.: Variational Analysis. 2nd edn. Springer (2009)
13. Zeidler, E.: Nonlinear Functional Analysis and its Applications: Fixed Point Theorems. Volume I. Springer (1993)
14. Grant, M., Boyd, S.: CVX: Matlab Software for Disciplined Convex Programming, version 2.1. http://cvxr.com/cvx (March 2014)